3D FLIP-UP STRUCTURE OF POROUS SILICON WITH ACTUATOR AND OPTICAL FILTER FOR MICROSPECTROMETER APPLICATIONS

G. Lammel and P. Renaud
Swiss Federal Institute of Technology Lausanne (EPFL), Institute of Microsystems (DMT IMS)
CH-1015 Lausanne, Switzerland
Tel. ++41 21 693 6573, Fax. ++41 21 693 5950, e-mail: Gerhard.Lammel@epfl.ch

ABSTRACT

This paper reports a new fabrication method for a microactuated tunable optical filter based on porous silicon formation followed by electropolishing. This surface micromachining process generates in a single step a multilayered optical interference filter, releases it from the substrate and lifts it out of plane [1]. The filter can be tilted by a thermal bimorph actuator in order to tune the wavelength it transmits or reflects. The fabrication process uses only two photolithography levels on ordinary silicon p^+ substrates. Large, flat, actuatable flip-up Bragg mirrors of porous silicon have been realized with a typical thickness of 30 µm and areas ranging from 250 µm by 750 µm to 2400 µm by 4000 µm. Their capability to distinguish light sources with a wavelength separation of less than 20 nm in the visible is presented.

INTRODUCTION

Porous silicon formed by electrochemical etching in hydrofluoric acid (HF) has gained a lot of attention in the recent years as a photoluminescent material [2] and for sacrificial layers in MEMS [3]. It is rarely used as constitutive material for microstructures. In this paper, porous silicon is presented as a suitable material for free-standing micromirrors and optical filters, generated efficiently by a surface micromachining process without the use of sacrificial layers. Electropolishing of silicon at high current densities is used to detach the micro-structure from the substrate. The combination of macro pore generation in silicon and electropolishing was already reported elsewhere as a fabrication process for a suspended mass an accelerometer [4]. However, that structure does not move out of plane and cannot be actuated.

A multilayered dielectric optical interference filter of porous silicon is based on the effect that the index of refraction of every layer is given by its porosity, which can be adjusted by the current density during the electrochemical etching process [5]. This allows integration of optical elements for visible and infrared light in a free-standing plate without additional fabrication steps.

Two thermal bimorph actuator arms hold the optical element and can tilt it with respect to the substrate. The variation of the incident angle of light shifts the spectrum of the optical interference filter according to Bragg's law.

FABRICATION PROCESS

Electrochemical etch cell

For the porosification and electropolishing of silicon wafers, a so-called electrochemical double-cell was used (Fig. 1). It contains two platinum electrodes, one in each part of the cell, with the wafer in the middle,

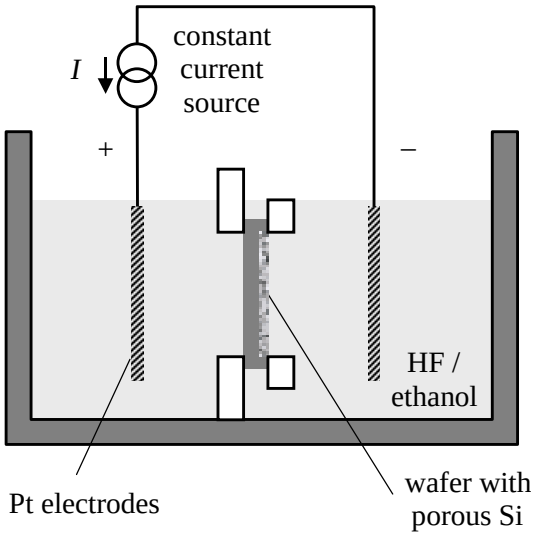

Fig. 1: Electrochemical etch cell for porosification and electropolishing of silicon wafers

completely separating the two parts. The current is forced to pass through the wafer, etching its anodic side. The p^+ doped wafer makes an ohmic contact with the electrolyte. The uniformity of this process is better than with single cells, which need a metallic backside contact. The etch bath can be stirred to improve homogeneity. A standard electrolyte consisting of HF 50% wt. and ethanol in a volume ratio of 1:1 was used.

Mask technology

To define the regions to be porosified or electropolished on the silicon substrate, different types of etch masks can be used [3, 6, 7]. Photoresist masks dissolved in standard HF electrolyte within minutes and did not give satisfactory results. Therefore, silicon nitride (Si_3N_4, low stress, LPCVD deposited, 500 nm thickness) was used. The Si_3N_4 mask resists the HF electrolyte for about one hour.

On top of this Si_3N_4 mask, a metal layer was evaporated to create a thermal bimorph heater. An 800 nm Au layer with a 10 nm Cr adhesion layer worked fine and resisted HF; an evaporated Cr/Ni layer gave good results, too. Metal tracks and bond pads were structured by standard photolithography and a wet etch process. Then the Si_3N_4 mask underneath was dry etched in SF_6 using standard photolithography. Fig. 2 illustrates the wafer with two mask levels, ready to be porosified.

Formation of porous silicon

In order to obtain mesoporous silicon that is more stable mechanically than electroluminescent nanoporous silicon, highly doped p^+ silicon substrates with a resistivity of 0.01 • cm were used. The electrochemical etch bath was driven by a computer-controlled constant

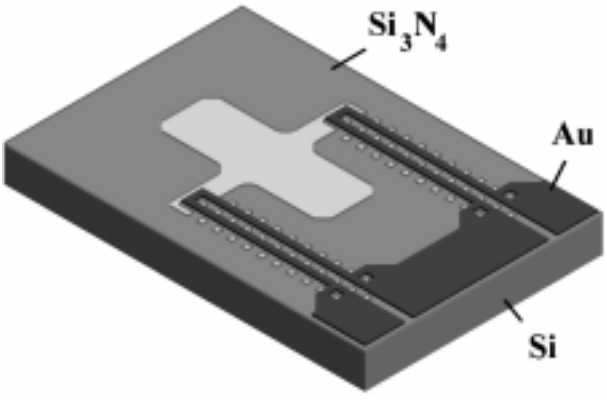

Fig. 2: The silicon wafer with two mask levels, prepared to be electrochemically etched. The silicon nitride defines the area of the flip-up plate. The gold tracks on top serve as heater wires for a thermal bimorph actuator.

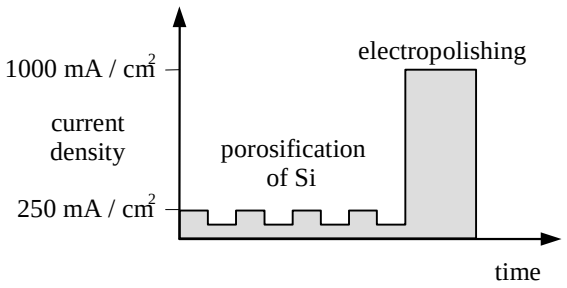

Fig. 3: Schematic diagram of current densities during the phases of porosification and electropolishing of silicon.

current source with no additional reference electrodes. The current source was programmed to deliver a modulated current density of 100 to 250 mA / cm^2 (calculated per open mask area) for some minutes to form the porous silicon layer of desired thickness with the integrated optical interference element (Fig. 3). Current density modulation created a porosity layer profile that corresponds to the desired profile of index of refraction of the optical interference filter. Since the electrochemical etching only takes place at the interface between porous silicon (filled with electrolyte) / bulk silicon, the density at any depth can be adjusted individually without influencing the layer stack already formed. Typical etch rates are 100 nm / sec at a porosity of 50 %. In a more precise calculation, one can take into consideration that the effective etch interface area increases because of the mask underetch, leading to a ramp for the total current. This is important for accurate optical elements.

Electropolishing

Directly after porosification, the current density was increased to 1 A / cm^2 to switch to electropolishing, etching the silicon below the porous layer at a typical rate of 310 nm / sec. This step substitutes the use of a sacrificial layer in classical surface micromachining and detaches the porous layer from the substrate. The cross-section of the structure under a mask opening resulting from this process is illustrated in Fig. 4. Current coming from the backside plane is forced to squeeze through the mask opening, leading to a local lateral current flow. The current density is increased at the sides of the mask openings and the lateral underetch is nearly isotropic. As a consequence of the lateral current, the electropolishing also releases the sidewalls of the porous layer. The thickness of the separation gap can be adjusted by the electropolishing time.

After electropolishing, the plate of porous silicon is still held by the Si_3N_4 mask at the underetched border zone. It can be released by dissolving the mask, so the wafer was left in the HF / ethanol bath for about 30 minutes

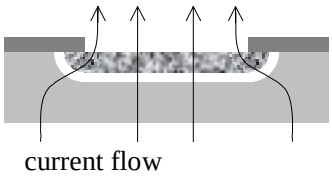

Fig. 4: Formation of porous silicon with subsequent electropolishing gap formation, structured using an insulating mask. Lines of electrical current flow are indicated.

after the electrochemical etch process had finished. The whole etching process takes less than one hour.

Suspension by actuator arm

For suspended microstructures it may be desirable to release a plate from some sides but hold it at defined points. This can be achieved by perforating the Si_3N_4 mask in a region that serves as suspension arms with square holes of typical dimensions 20 µm sidelength and 50 µm period (Fig. 5). An isotropic etch creates a field of bumps of porous silicon under the perforated region. They will be linked when the lateral underetch of two adjacent holes meets and forms the suspension arms. The average current density at the porous silicon / bulk silicon interface under a perforated region is lower than in regions where the mask is completely open. This makes the suspension arms thinner and more flexible than the plate to be suspended.

The arms were made actuatable by the metal tracks on top of the Si_3N_4 mask between the perforation holes. The tracks serve as resistive heaters for the thermal

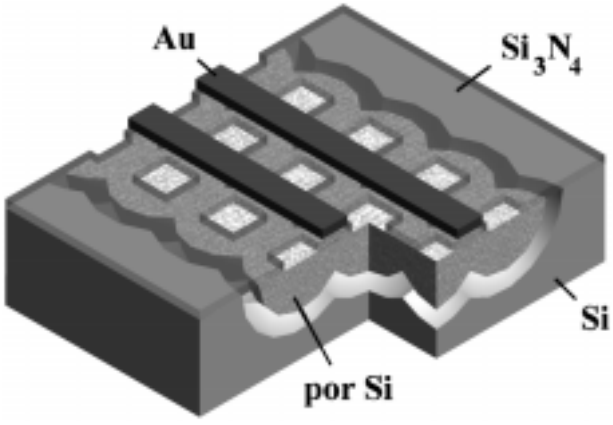

Fig. 5: Section of the actuator arm after the electrochemical etching process. The porous silicon is released from the substrate but still held by the Si_3N_4 mask, here shown transparent. Typical dimensions of Si_3N_4 openings: 20 µm x 20 µm, Au tracks: 20 µm width.

bimorph. At the same time they link the end of the arm to the substrate like a bridge. The Si_3N_4 under it is protected and is not dissolved during the mask stripping.

Drying

After the wafer is removed from the electrolyte bath, it is rinsed in water for about 15 minutes. Drying the free-standing structure is a delicate step. Using a spinner or a nitrogen gun would damage the structures, so it is dried in air. To prevent sticking from surface tension, the separation gap between the porous silicon and the substrate was etched at least 20 µm deep by choosing the electropolishing time. Substituting the water with isopropanol lowered the surface tension and improved drying.

Oxidation and lift-up

The porous silicon can be partly oxidized in oxygen plasma. The implanted oxygen atoms create a compressive strain gradient in the suspension arms and make the plate lift up out of plane (Fig. 6). This can be explained in the following way: In the perforated zone, the current is squeezed through the perforation holes. At the beginning of the porosification the current density is higher than at the end, when the current is distributed over the whole area. As the porosity increases with current density, the suspension arm is more porous on the top than at the bottom. This means that during oxidation, the bottom part expands more strongly by the integration of oxygen atoms [8] than the top, leading to more compressive stress on the bottom, which finally

Fig. 6: SEM picture of a free-standing, mobile, flat plate of density modulated porous silicon lifted out of plane by two actuator arms. The plate contains 256 double layers with high and low indices of refraction.
Dimensions: 1100 µm x 1850 µm x 30 µm.

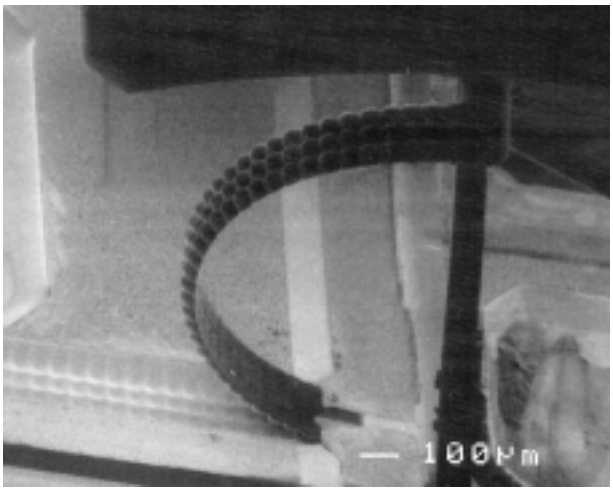

Fig. 7: SEM picture of the actuator arm holding the free-standing plate of Fig. 6 after complete oxidation (detail). The plate is turned over by 180° and is only partly shown on the top of the picture. Note the ripples resulting from the perforated mask.

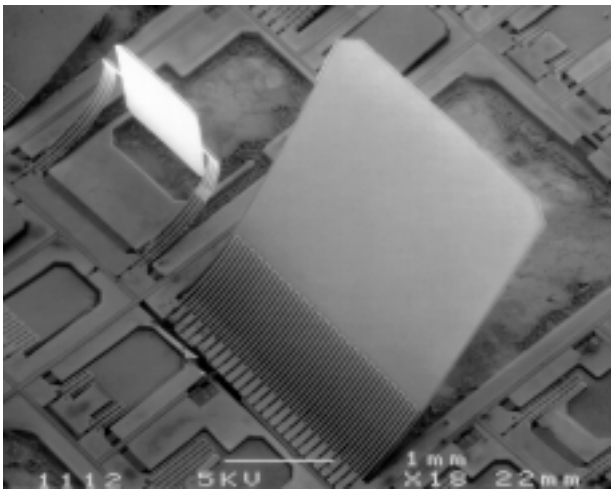

Fig. 8: SEM picture of a large free-standing, mobile, flat plate of density modulated porous silicon lifted out of plane by a ribbon actuator. Dimensions: 2570 µm x 3000 µm x 30 µm,

lifts up the plate. This stress-induced lift-up is amplified by the metal layer on the Si_3N_4. A layer of Cr and Au deposited by evaporation will contract at room temperature, create a contractile stress on the top and help to pull up the plate when it is released.

Porous silicon oxidizes rapidly even at room temperature because of its vast internal surface area of up to 600 m^2 per cm^3 [2]. To prevent an aging effect resulting in a shift of the rest position of the plate, porous silicon can be pre-aged by complete oxidation. It can be converted to porous SiO_2 within 60 minutes at 950°C under water vapor atmosphere (Fig. 7). This lowers the index of refraction considerably and makes the material transparent to visible light.

RESULTS

Large, flat, flip-up optical interference filters of porous silicon were realized with a typical thickness of 30 µm and areas ranging from 250 µm by 750 µm to 2400 µm by 4000 µm (Fig. 6, 7, 8). In the rest position, they are lifted by two arms 10° to 90° out of plane. Experiments with different thicknesses show that the plate begins to curve when it is thinner than 15 µm and is difficult to lift up when it is thicker than 40 µm. The alternative design in Fig. 8 uses a suspension ribbon instead of two arms. This geometry leads to lower rest and dynamic angles, but is less fragile when large plates are required.

Actuator

The filter plates can be thermally actuated by applying up to 5 Volts. Power consumption is about 100 mW. Because the thermal expansion coefficient of the metal is higher than that of Si_3N_4 on porous Si or porous SiO_2, the actuator arm bends down when switched on. Fig. 9 shows the dependence of tilt angle on DC input voltage. These and the following measurements were taken with a test set-up consisting of a laser beam pointing at the filter, a position sensitive detector to measure the angle

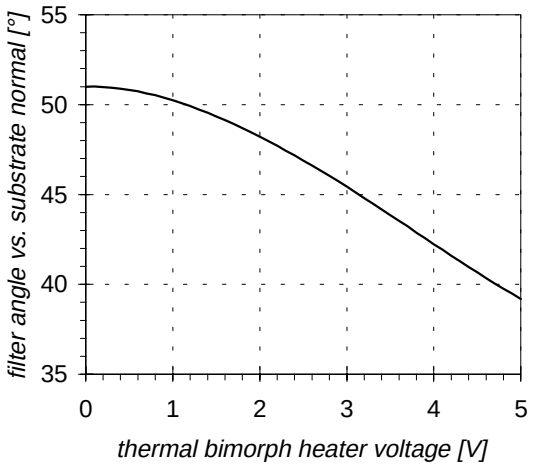

Fig. 9: Tilt angle of the optical filter plane in dependence of the actuator DC voltage. The behaviour is first quadratic as the temperature goes with the heating power, then flattens out because of a change of the resistance and the elastic constants with temperature.

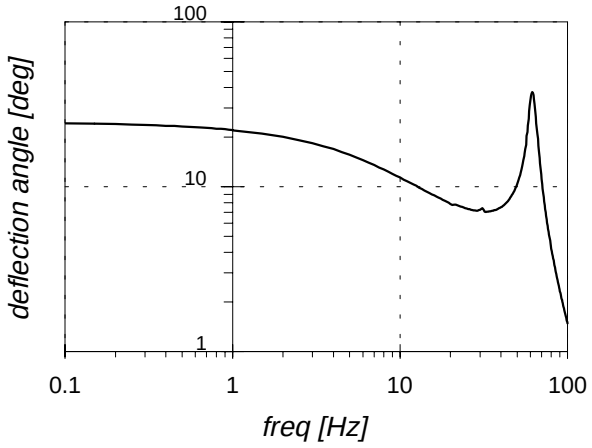

Fig. 10: Frequency plot of the amplitude of optical deflection of a filter plate driven by the bimorph actuator. The thermal cut-off frequency is 9 Hz, the meachnical base resonance frequency is 61.1 Hz with a FWHM (full width at half maximum) of 10.1 Hz.

of reflection and its intensity as well as a data acquisition computer.

Thermal cut-off

The bimorph actuator can be heated quickly, but cooling down is the speed-limiting factor. The cut-off frequency varies with the design geometry and material; values from 9 Hz to 500 Hz were found (Fig. 10). The fact that Ni heaters have generally a lower cut-off frequency than Au heaters shows that cooling is mainly given by the heat conductivity of the metal tracks into the substrate, and that convection and radiation does not play a significant role.

Mechanical resonance

The filter plate can be set into mechanical resonance, similar to the barcode scanner reported elsewhere [9]. Depending on geometry, the fundamental frequency lies between 60 and 3000 Hz (Table 1). The angle of rotation can be as large as 30° at resonance. Stroboscopic illumination reveals that the movement at resonance - far beyond the thermal cut-off - is different from the DC movement. Only the ends of the actuator arms close to the substrate flex. This is the only place where the heat can be dissipated fast enough; the rest of the actuator arms is always at a nearly constant temperature and does not contribute to the movement. Higher order modes up to 7000 Hz with mode shapes different from the base mode have been observed, e.g. an antiparallel torsion movement of the plate and the arms.

Spectrometer application

With conventional layer stacks for interference filters, the choice of index of refraction is generally restricted by the materials used. Porous silicon allows gradual index profiles, which offer more design freedom e. g. Rugate filters. Fig. 11 shows the reflectivity spectrum of a Bragg reflector of oxidized porous silicon at normal incidence, containing 183 periods with sinusoidal modulation of the index of refraction between 1.31 and 1.42. The center wavelength decreases for gracing incidence. This means that tuning the filter by tilting it can scan the spectrum.

Table 1: Measured fundamental resonance frequencies of suspended plates of porous silicon in bending mode for some different geometries and suspension types.

plate dimensions	suspension type	suspension length	resonance frequency
580 x 800 μm^2	2 arms	720 µm	1100 Hz
580 x 620 μm^2	2 arms	1100 µm	567 Hz
1100 x 1850 μm^2	2 arms	1680 µm	207 Hz
400 x 640 μm^2	ribbon	280 µm	1172 Hz
620 x 820 μm^2	ribbon	330 µm	584 Hz
2570 x 3000 μm^2	ribbon	960 µm	61 Hz

To demonstrate the incidence angle dependent wavelength selection, the following experimental set-up was used: LED's with colors from 592 nm (amber) to 635 nm (red) peak wavelength, 17 nm spectral halfwidth and 6° viewing angle pointed parallel to the substrate at the tunable Bragg mirror of porous silicon. The angle of reflection and the reflected intensity were simultaneously recorded during a sweep of the actuator voltage from 0 to 5 volts (Fig. 12). The intensity was corrected for the projected area of the mirror and the different brightness' of the LED's. The plot shows that the wavelength resolution is better than 20 nm. The peak is smeared out because of inhomogeneities of the

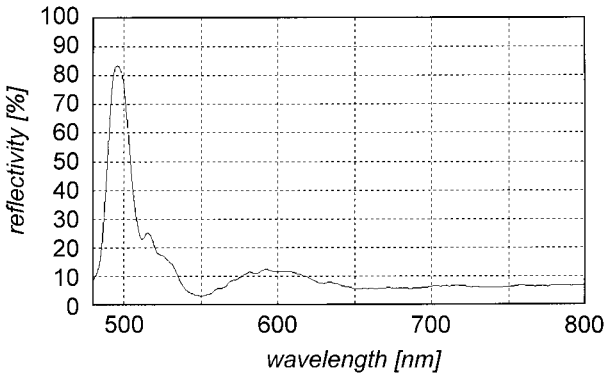

Fig. 11: Reflectivity spectrum of a Bragg reflector of oxidized porous silicon at normal incidence.

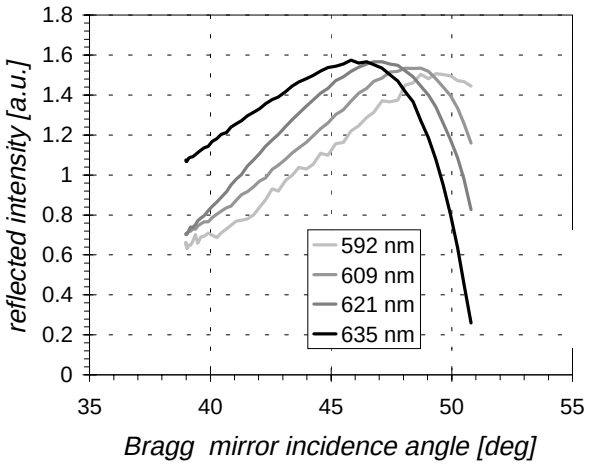

Fig. 12: Intensity reflected by a tunable Bragg mirror for different LED light sources. The wavelength can be selected by the incidence angle (equals the exit angle).

porous silicon layer thickness due to current inhomogeneities during the etch process. In future designs this effect will be minimized by an improved mask geometry that equalizes the current density distribution better.

Besides Bragg mirrors (band reflectors), tunable Fabry-Perot filters (bandpass in transmission) are possible. A spectrometer can be built with only one detector pixel behind this filter, in contrast to conventional grating or prism spectrometers that need a linear detector array.

CONCLUSION

A new technology that combines porous silicon layers and sub-surface electropolishing is presented. It allows the fabrication of three-dimensional flip-up microplates of porous silicon of up to 50 µm thickness and several mm^2 in size. They can be actuated by a thermal bimorph. Optical elements can be easily integrated to obtain wavelength tunable filters and tunable color mirrors. Only one surface micromachining process step is needed while using standard wafers. It was demonstrated that these devices are capable of selecting wavelengths in the visible with a resolution of better than 20 nm. This opens up promising applications in micromechanics and microoptics such as micro-spectrometers for visible and infrared light.

ACKNOWLEDGMENTS

This work was funded by the Swiss Federal Institute of Technology Lausanne (EPFL). Silicon processing was done at the EPFL Center for Microtechnology (CMI).

REFERENCES

[1] European patent application 99117852.6, G. Lammel, "Procédé de fabrication d'une microstructure intégrée suspendue tridimensionelle, microstructure intégrée notamment obtenue par ce procédé et élément optique intégré réglable", 1999.

[2] A. G. Cullis, L. T. Canham and P. D. J. Calcott, "The structural and luminescence properties of porous silicon", *Journal of Applied Physics*, Vol. 82 (3), 1997, p. 909-965.

[3] A. P. Steiner and W. Lang, "Micromachining applications of porous silicon", *Thin Solid Films*, Vol. 255, 1995, p. 52-58.

[4] H. Ohji, P. T. J. Gennissen, P. J. French, K. Tsutsumi, "Fabrication of Accelerometer using Single-Step Electrochemical Etching for Micro Structures (SEEMS)", *IEEE International Micro Electro* Mechanical Systems (MEMS) Conference, Orlando, 1999.

[5] U.S. patent 5,696,629, M. G. Berger, H. Münder, S. Frohnhoff, M. Thönissen, H. Lüth, "Optical component comprising layers of porous silicon", 1997.

[6] M. Krüger, R. Arens-Fischer, M. Thönissen, H. Münder, M. G. Berger, H. Lüth, S. Hilbrich, W. Theiss, "Formation of porous silicon on patterned substrates", *Thin Solid Films*, Vol. 276, 1996, p. 257-260.

[7] G. Kaltsas, A. G. Nassiopoulou, "Frontside bulk micromachining using porous-silicon technology", *Sensors and Actuators A*, Vol. 65, 1998, p. 175-179.

[8] J. J. Yon, K. Barla, R. Herino, G. Bomchil, "The kinetics and mechanism of oxide layer formation from porous silicon formed on *p*-Si substrates", *Journal of Applied Physics*, Vol 62 (3), 1987, p. 1042-1048.

[9] S. Schweizer, S. Calmes, M. Laudon and Ph. Renaud, "Thermally actuated optical microscanner with large angle and low consumption", accepted for *Sensors & Actuators A*.